AERODYNAMIC MODELLING OF AN ACTIVE FLOW CONTROL SYSTEM FOR FLAPLESS FLIGHT CONTROL IN THE PRELIMINARY DESIGN STAGES

Korbinian Stadlberger* and Mirko Hornung†

Technische Universität München, Institute of Aircraft Design

Boltzmannstr. 15, 85748 Garching bei München, Germany

A modelling method is presented that translates the two-dimensional aerodynamics of active flow control aerofoils into an aerodynamic data set of a three-dimensional finite wing. The assembly of a 2D data set through automated RANS calculations of a Coandă flap concept forms the basis for the subsequent extrapolation on the finite wing by means of the proposed "cambering" method. The iterative procedure is based on potential theory and modifies the implied vortex lattice by locally tilting the normal vectors on the collocation points to match the local aerodynamic reactions given by the viscous RANS aerofoil data. In the context of preliminary aircraft design this computationally efficient method leads to an aerodynamic data module that contains the 3D aerodynamic reactions due to Coandă flap actuation. In this study the method is applied on a low aspect ratio wing.

Nomenclature

α_∞	=	free stream angle of attack	[°]	C_l	=	wing roll moment coefficient	[-]
α_{loc}	=	local angle of attack at wing section	[°]	c_l	=	section lift force coefficient	[-]
β_∞	=	free stream sideslip angle	[°]	C_m	=	wing pitching moment coefficient	[-]
δ_1, δ_2	=	local lattice modification angles	[°]	c_m	=	section pitching moment coefficient	[-]
η	=	plain flap deflection angle	[°]				
η_h	=	outflow momentum ratio based on slot heights	[-]	C_μ	=	jet outflow momentum flux coefficient, $C_\mu = \frac{U_{jet}\dot{m}_{jet}}{\frac{1}{2}\rho U_\infty^2 S_{ref}}$	[-]
$\varphi_{0\%}$	=	leading edge sweep angle	[°]	c_{avg}	=	mean geometric wing chord, $c_{avg} = \frac{S_{ref}}{b}$	[m]
AR	=	wing aspect ratio	[-]				
b	=	wing span	[m]	C_T	=	thrust effect coefficient	[-]
c	=	wing section chord length	[m]	h_{total}	=	total slot height, $h_{total} = h_{upper} + h_{lower}$	[m]
C_D	=	wing drag force coefficient	[-]				
c_d	=	section drag force coefficient	[-]	r	=	radius of Coandă surface	[m]
C_L	=	wing lift force coefficient	[-]	U_∞	=	free stream velocity	[-]
				U_{jet}	=	mean jet outflow velocity	[-]

1 INTRODUCTION

In the framework of the German national research program SAGITTA novel solutions for flapless flight control effectors are subject of investigation [1]. In terms of low observability and maintenance cost it is of interest to avoid gaps between conventional flaps and to reduce the number of moving parts. For highly dynamic control manoeuvres blown circulation control aerofoils are able to provide the required control moments without any of the complex kinematics as conventional flaps would imply [2–6]. Blowing over a rounded Coandă trailing edge entrains the baseline airflow around the aerofoil to the desired direction and modifies the section circulation strength (see Fig. 1). Basically this system exhibits aerodynamic similarities as conventional flaps where the momentum vector is bended upwards or downwards. The scope of the research activities on this flapless flight control concept is primarily the applicability on low aspect ratio flying wing configurations (e.g. $AR < 3$, $\varphi_{0\%} > 50°$). These might even be designed laterally unstable for low observability reasons (see Fig. 3) and in general imply particular challenges [7]. Here, the current concept promises to be suitable also for yaw control when air flow momentum is controlled differentially on the wing half spans. In service the

---

*Research Engineer, Technische Universität München, Institute of Aircraft Design.
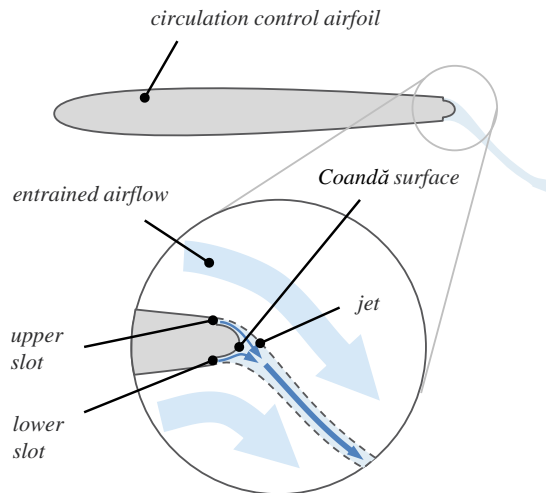†Professor, Technische Universität München, Institute of Aircraft Design.

Figure 1: Illustration of Coandă aerofoil with double-slotted blowing
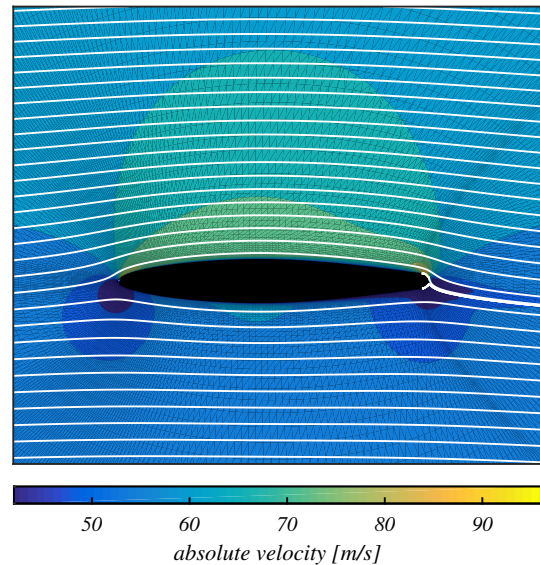

Figure 2: Exemplary 2D flow field from numerical simulation, $\frac{r}{c} = 0.02$, $\frac{h_{total}}{r} = 0.05$, $\frac{U_{jet}}{U_\infty} = 3$, $\eta_h = 0.8$, $\alpha_\infty = 0°$

double-slotted Coandă flaps with independently controllable slot heights will have to provide the necessary mix of control moments around all three axes. Therefore an aerodynamic data model has to be set up to evaluate the aerodynamic effectiveness of a given Coandă flap system design as a function of control factors. Especially for preliminary design stages computational efficiency and flexibility in terms of parameter variation are crucial. For this the proposed method allows to evaluate the investigated type of flow control concept for a still pending aircraft configuration. During the preliminary design stages of an aircraft system large numbers of parameter variations are of interest. Not only the separate optimisation of the subsystems benefit from the exploration of the design space but also the multidisciplinary design process of the global system can be supported by quick and robust performance estimation methods. Especially the prediction of aerodynamic reactions raises challenges when computational efficiency and accuracy still seem to be contradictory. The combination of two-dimensional wing section data predicted by Reynolds Averaged Navier-Stokes (RANS) calculations and its subsequent extrapolation on the finite wing based on potential theory depict a compromise suitable for preliminary design.

In this article the focus is set on the extrapolation of 2D aerofoil data to 3D finite wing data. The first section describes briefly the automated RANS calculation tool for 2D data generation, defines the necessary blowing and control parameters and presents an excerpt of the 2D data set that was assembled after a calculation campaign. The subsequent section contains the governing equations and detailed sequence of the proposed 3D extrapolation method that relies on potential theory and computes the complete three-dimensional re-actions of the finite wing based on the viscous 2D section data. Comparative calculations on wind tunnel experiments of finite wings with conventional plain flaps validate the method's applicability on low aspect ratio wings. The last section finally presents the combined results of 2D RANS aerofoil data and proposed cambering method for the studied SAGITTA wing.

2   CALCULATION METHOD FOR WING SECTION AERODYNAMICS (2D)

The two-dimensional aerofoil section data (c_l, c_d, c_m) forms the basis for the control force and moment es-timation of the entire wing (C_L, C_D, C_Y, C_m, C_n, C_l). Although numerous wind tunnel experiments have been performed on active flow control and Coandă flaps [2–6] there is no systematically collected data or accu-rate empirical correlation available that enables the aerodynamic modelling of an arbitrary Coandă aerofoil shape. Therefore an automated approach incorporating computational fluid dynamics (CFD) was chosen for the modelling of the diffusion, i.e. viscosity driven flow problem where 2D potential theory methods natu-rally fail. Even if the accurate prediction of Coandă flap effectiveness poses challenges under conditions of strong blowing through one single slot [9] the implemented RANS method is supposed to provide reliable re-sults for large portions of the operational area where double-slot-blowing prevails. The following subsections briefly describe the implemented tool and present an excerpt of a 2D data set that was generated during a
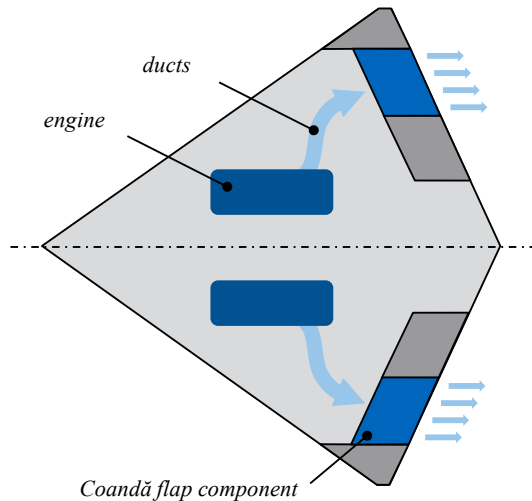
Figure 3: Illustration of studied low aspect ratio wing configuration with Coandă flap system
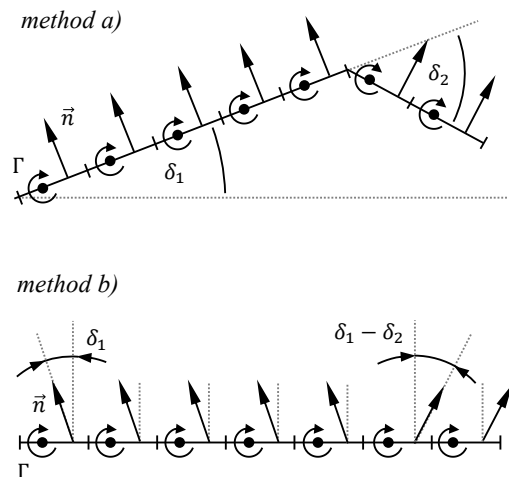
Figure 4: Panel modification method a) of ref. [8] and present method b)

calculation campaign and is used for the subsequent extrapolation on the finite wing.

2.1 RANS Calculation Tool (2D)

For the estimation of attainable forces and moments (c_l, c_d, c_m) in the two-dimensional case the steady incompressible RANS equations are solved by the finite volume method inside the MATLAB environment. The current implementation includes the hybrid differencing scheme which combines both upwind and central differencing scheme [10]. In order to avoid a non-physical discretisation induced "checker-board" pressure field a staggered grid approach for velocity components and scalar parameters has been carried out [11]. For the computation of velocity and pressure a coupled solver strategy was chosen which solves the momentum and continuity equations simultaneously inside one system of linear equations. Turbulence modelling is provided by a segregated solution approach of Menter's two-equation k-ω-model with shear stress transport (SST) [12].

Furthermore several automated features have been introduced as the tool is intended to be used for large calculation campaigns on several desktop machines or cluster systems including widespread parameter variations. An automated mesher with algebraic initialisation and subsequent orthogonalisation through elliptic solver creates a grid on the basis of given baseline aerofoil coordinates, trailing edge radii and nominal slot heights. In order to increase robustness and convergence rate at the beginning of the iterative calculation process the flow field is initialised by an approximated inviscid solution evolving from potential theory. Finally, an automated calculation campaign for several operation points can be launched once the free stream and blowing properties are specified. A convergence detection, that monitors the lift coefficient evolution, enables the premature completion of each single calculation leading to significant time savings.

2.2 Aerofoil Section Results (2D)

The calculations in the scope of this study were performed on in-house desktop machines equipped with Intel Core i7-4770 processors (quad core à 3.40Ghz) and 8GB RAM. One iteration took between 5s and 10s where a converged lift coefficient was attained after 40 to 80 iterations in the majority of cases. Several parameter variations (e.g. Coandă radius, slot heights, blowing velocity etc.) have been investigated during an automated calculation campaign on 18 quad-core desktop machines enabling a total number of 72 simultaneous simulations. Hence, the results of 30,000 calculated data points can be extrapolated on the finite wing in a subsequent step (section 3) to obtain the 3D reactions for the given wing planform. After a short introduction of relevant flow parameters some exemplary results will be presented in this subsection.

In literature it is common to describe the aerodynamic force and moment reactions dependent on the normalised momentum flux of the outflow, i.e. the equivalent thrust force. The flow momentum coefficient C_μ
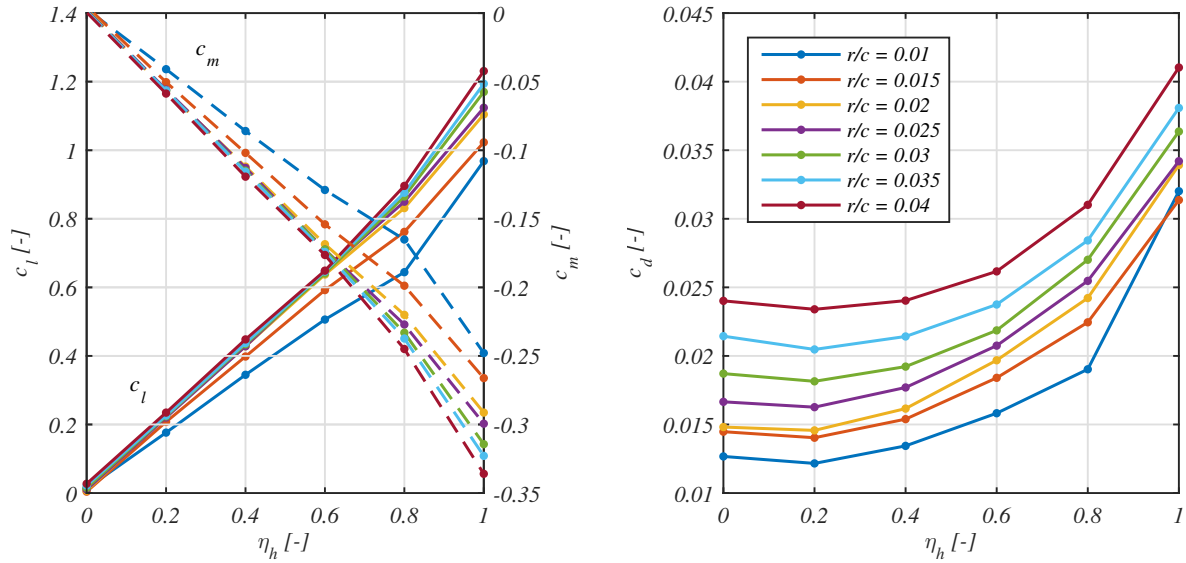
Figure 5: Coandă aerofoil section aerodynamics over η_h for different Coandă surface radii $\frac{r}{c}$, $\frac{h_{total}}{c} = 0.001$, $\frac{U_{jet}}{U_\infty} = 3$, $\alpha_\infty = 0°$

therefore yields

$$C_\mu = \frac{\dot{m}_{jet} U_{jet}}{\frac{1}{2}\rho_\infty U_\infty^2 S_{ref}} \tag{1}$$

where $\dot{m}_{jet}$ is the jet mass flow, U_{jet} the jet outflow velocity, $\frac{1}{2}\rho_\infty U_\infty^2$ the free stream dynamic pressure and S_{ref} the lifting surface reference area. The investigated concept of a circulation control aerofoil features both an upper and lower slot which are supplied by one common plenum chamber imposing one total pressure value. Thus, the momentum flux coefficients $(C_\mu)_{upper}$ and $(C_\mu)_{lower}$ of the upper and lower slot can be controlled by adjusting their respective slot heights. For the following analysis of the results a new control parameter η_μ is defined which is meant to be equivalent to a plain flap deflection ranging from -1 (flap deflected 100% upwards) to 1 (flap deflected 100% downwards). It yields

$$\eta_\mu = \frac{(C_\mu)_{upper} - (C_\mu)_{lower}}{(C_\mu)_{upper} + (C_\mu)_{lower}} \tag{2}$$

and can be approximated by the following expression

$$\eta_\mu \approx \eta_h = \frac{h_{upper} - h_{lower}}{h_{total}} \tag{3}$$

where $h_{total} = h_{upper} + h_{lower}$. Again, the control parameter η_h spans the operational range from the cases of completely closed upper slot ($h_{lower} = h_{total}$; $\eta_h = -1$) to completely closed lower slot ($h_{upper} = h_{total}$; $\eta_h = 1$).

Fig. 5 shows the two-dimensional aerodynamic reactions (c_l, c_d, $c_{m_{25\%}}$) of a double-slotted Coandă aerofoil at zero angle of attack ($\alpha_\infty = 0°$) whose aerofoil shape was derived from the NACA 64-A012 aerofoil (Fig. 2). The shared plenum is pressurised such that the jet outflow velocity ratio $\frac{U_{jet}}{U_\infty}$ reaches a value of 3. Except at high slot ratio values η_h (where the lower slot is nearly closed) the lift and pitching moment coefficients exhibit an approximately linear behaviour with increasing values of the control factor η_h for all Coandă-radius-to-chord-ratios $\frac{r}{c}$. Moreover Coandă flap effectiveness ($\frac{\partial c_l}{\partial \eta_h}$, $-\frac{\partial c_m}{\partial \eta_h}$) grows with increasing Coandă radius. However, the effectiveness gain seems to saturate at a radius-to-chord-ratio of approx. $\frac{r}{c} = 0.02$. Aerofoil section drag decreases slightly until $\eta_h = 0.2$ before it disproportionately rises to its maximum value at $\eta_h = 1$. In general, drag grows with increasing Coandă radius. Note that the section drag coefficient c_d only includes the integrated friction and pressure forces acting on the aerofoil and Coandă surface skin. The thrust force effect through blowing is not added. Fig. 6 shows the section aerodynamics with varying total slot height h_{total}. Higher total-slot-height-to-chord-ratios lead to an increased Coandă flap effectiveness ($\frac{\partial c_l}{\partial \eta_h}$, $-\frac{\partial c_m}{\partial \eta_h}$), however, effectiveness gain seems to be limited and once more exhibits a saturated behaviour for higher total slot
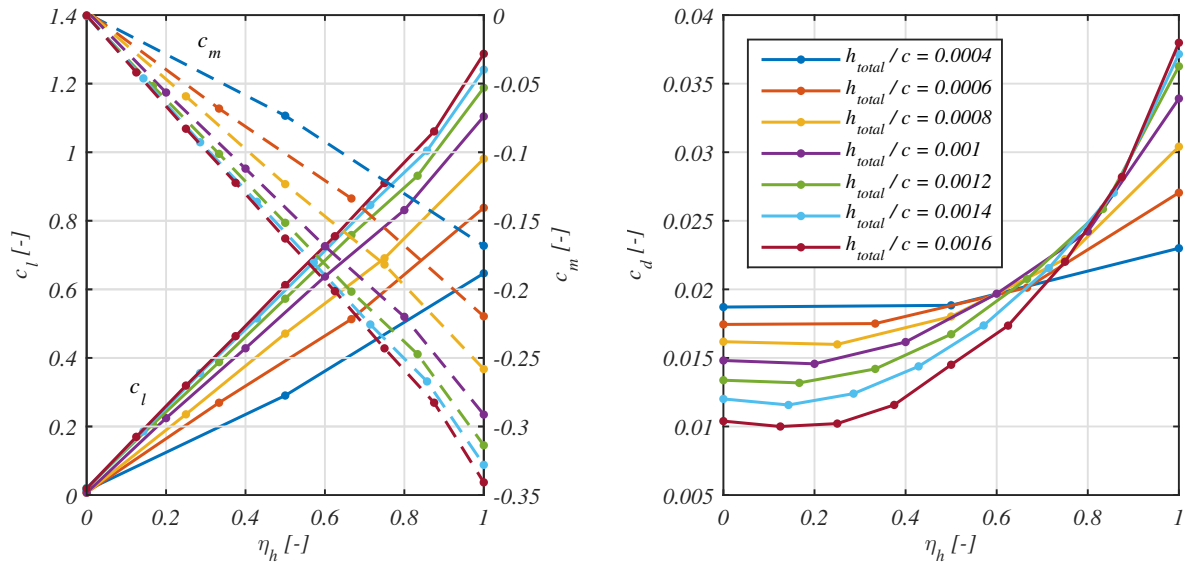
Figure 6: Coandă aerofoil section aerodynamics over η_h for different total slot heights h_{total}, $\frac{r}{c} = 0.02$, $\frac{U_{jet}}{U_\infty} = 3$, $\alpha_\infty = 0°$

heights. In addition, section drag is visibly dependent on total slot height, i.e. total jet mass flow. High total-slot-height-to-chord-ratios lead to decreased drag for low control factors η_h while section drag raises at high values of η_h and increasing total slot heights.

3 CALCULATION METHOD FOR FINITE WING AERODYNAMICS (3D)

The combination of two-dimensional wing section data predicted by RANS calculations and its subsequent extrapolation on the finite wing by the incorporation of potential theory was chosen as appropriate method to meet both requirements of sufficient accuracy and computational efficiency (w.r.t. the present standard of available CPU power). Linear methods as Prandtl's Lifting Line Theory [13] or the Vortex Lattice Method (VLM) [14] give reliable results for a finite wing if the aerofoil section can be expected to produce the theoretical lift force of an inviscid flat plate ($c_{l_\alpha} = \frac{\partial c_l}{\partial \alpha} = 2\pi$) throughout the investigated angle of attack range. However, viscous effects leading to non-linear polars for lift and pitching moment are not taken into account by the pure potential theory. Here, iterative approaches have been developed to introduce real section data into the solution process to model stall phenomena and low Reynold's number effects [15, 16]. The modern adaptions of the lifting line method use discrete horseshoe vortices and iteratively adjust the collocation point position, i.e. the lift curve slope (c_{l_α}), according to viscous aerofoil data and local angle of attack [17]. However, the estimation of the 3D moment and force reactions on a low aspect ratio wing additionally requires the modelling of circulation strengths in the chordwise direction (see Fig. 7). A vortex lattice more accurately accounts for cross flows due to low aspect ratios rather than a single lifting line. Therefore the vortex lattice method is more appropriate as theoretical basis for the studied flying wing configuration. The present "cambering" approach relies on the ideas of ref. [8] and iteratively introduces the non-linear section data into the solution of the discrete horseshoe vortex strengths. Mukherjee and Gopalarathnam used the expression "Decambering Approach" as wing sections are virtually "decambered" when flow separations occur in the post-stall region. Inside their method the vortex lattice is manipulated geometrically such that for the final solution the calculated values of local lift force and pitching moment coefficients ($c_l, c_{m,})_{pot}$ are consistent with viscous section data ($c_l, c_{m,})_{visc}$. After each iteration the discrete vortices are rotated around the leading edge and around a virtual flap hinge line to change the incidence and camber of each wing section (Fig. 4a). The rotation angles are determined by use of linearised analytical expressions that are derived from the classical solution of the lifting problem [18].

In the scope of the present research activities a new method is sought to incorporate the forces and moments generated by novel flight control technology rather than a technique to investigate the post-stall regime. Therefore the expression "cambering" approach was chosen for the following method as the aerofoil section is cambered through positive deflection of a plain flap or through an aerodynamically equivalent flight control effector, e.g. a Coandă flap. The following subsections describe the method used to establish a three-dimensional aerodynamic data set for the studied finite low aspect ratio wing. The algorithm was implemented
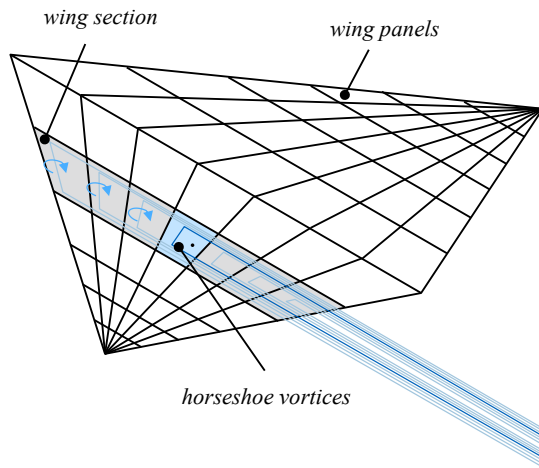
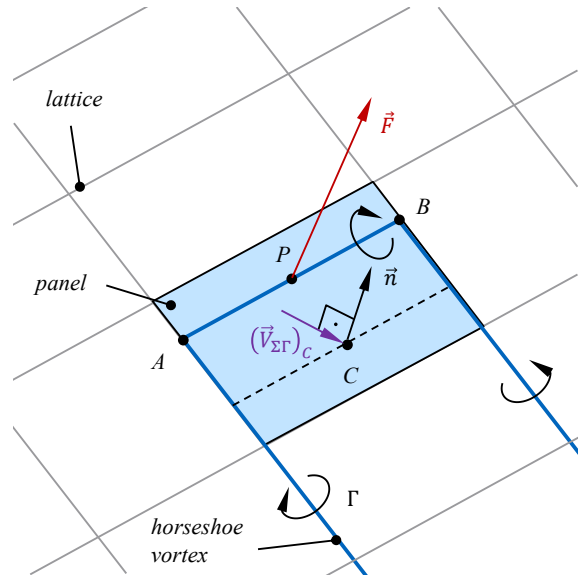**Figure 7: Illustration of vortex lattice for a low aspect ratio wing**

Figure 8: Illustration of horseshoe vortex

in MATLAB and is linked with an object-oriented parametric wing model enabling quick results for an arbitrary wing planform. The subsequent discussion of results from validating calculations assess the accuracy of the presented method.

3.1 Governing Equations

In the vortex lattice theory the lifting surface is divided into a discrete number of panels in both chordwise and spanwise direction (Fig. 7). In general the aerodynamics of the wing are modelled by a lattice of horseshoe vortices whose lateral filaments are placed on the panel quarter-chord-lines while the two associated longitudinal filaments are aligned to the freestream velocity and represent the wake sheet (see Fig. 8). The differential form of the Biot-Savart law can be integrated to yield the induced velocity $\left(\vec{V}_{\Gamma_j}\right)_C$ in point C of one of these vortex filaments j ranging from A to B

$$\left(\vec{V}_{\Gamma_j}\right)_C = -\frac{\Gamma_j}{4\pi} \cdot \frac{\vec{r}_{AC} \times \vec{r}_{BC}}{\left\|\vec{r}_{AC} \times \vec{r}_{BC}\right\|^2} \cdot \left[\left(\vec{r}_{AB}\right)^T \cdot \left(\frac{\vec{r}_{AC}}{\left\|\vec{r}_{AC}\right\|} - \frac{\vec{r}_{BC}}{\left\|\vec{r}_{BC}\right\|}\right)\right] \tag{4}$$

where Γ_j is the vortex strength of the vortex filament j. Hence, the velocity $\left(\vec{V}_{\Sigma\Gamma}\right)_{C_i}$ in point C_i induced by all N vortex filaments can be determined by

$$\left(\vec{V}_{\Sigma\Gamma}\right)_{C_i} = \sum_{j=1}^{N}\left(\vec{V}_{\Gamma_j}\right)_{C_i} + \vec{V}_\infty \tag{5}$$

where $\vec{V}_\infty$ is the free stream velocity. Then a Neumann boundary condition is established at all collocation points C_i that forces the flow velocity to be aligned with the respective panel surface, i.e. to be perpendicular to the normal vector $\vec{n}_{C_i}$. It yields

$$\left(\vec{V}_{\Sigma\Gamma}\right)_{C_i} \cdot \vec{n}_{C_i} = 0 \tag{6}$$

Note that the collocation points are located at the midpoint of the 3/4-chord line which theoretically results in a lift curve slope of $c_{l_\alpha} = 2\pi$ for one panel in the two-dimensional case. Finally the solution of the emerging system of linear equations (SLE) enables the determination of the vortex strengths Γ_j of each horseshoe vortex. The discrete forces $\vec{F}_i$ acting on the midpoints P of the lateral filaments AB can be calculated by use of the Kutta-Joukowski theorem

$$\vec{F}_i = \rho \cdot \Gamma_i \cdot \left(\left(\vec{V}_{\Sigma\Gamma}\right)_{P_i} \times \vec{r}_{AB}\right) \tag{7}$$

The global (C_L, C_D, C_Y, C_m, C_n, C_l) and local section values (c_l, c_d, c_m) of the force and moment coefficients are determined by integration and decomposition into the respective directions.

3.2 Calculation Procedure

The basic idea of the cambering or decambering approach is to change the camber and incidence of the vortex lattice such that the section lift force and pitching moment calculated by potential theory corresponds to the viscous aerofoil data at the estimated local angle of attack. The simplest practice is to introduce two angles δ_1 and δ_2 that model a simple flap (δ_2) for pitching moment generation and change the incidence of the entire wing section (δ_1) for lift force correction. Fig. 4a) illustrates a modified section according to the method used by ref. [8], where the vortices as well as collocation points and normal vectors are rotated (method a). However, for swept wings this method can induce non-physical lateral forces and moments if the virtual hinge lines are not perpendicular to the free stream direction. Therefore the present method only tilts the normal vectors to obtain the necessary local change in lift and pitching moment (method b). The details of the complete calculation procedure are described in the following paragraphs while the iterative process is additionally illustrated in Fig. 9.

Initial calculations:

As a matter of principle the following algorithm requires a correlation between the modification angles δ_1, δ_2 and their impact on the 2D section aerodynamics $(c_l)_{pot}, (c_m)_{pot}$. Mukherjee and Gopalarathnam used two linearised analytical expressions to calculate the two-dimensional reactions $(c_l)_{pot} = f_{analytical}(\delta_1, \delta_2)$ and $(c_m)_{pot} = f_{analytical}(\delta_1, \delta_2)$. As can be seen in Fig. 10 the linearised analytical solution deviates significantly from the 2D discrete vortex solution applying method a), especially at high deflection angles of δ_2. In fact, the investigated fluidic flight control concept promises very high lift increments leading to increasingly inaccurate solutions at high values of δ_1, δ_2. The deviation is even higher when solely the normal vectors are tilt as intended (method b). This proofs that the linearised approach is not valid anymore when high modification angles have to be expected. Hence, the two-dimensional reactions of the 2D baseline section have to be calculated with discrete vortices and stored in a look-up-table before the iteration process starts. Here, the 2D panel problem (Fig. 4b)) is solved for a fine grid of δ_1, δ_2-values. This subfunction inside the calculation tool is represented by $f_{2D\,panel}$ and provides

$$\left((c_l)_{pot}, (c_m)_{pot}\right)_{2D} = f_{2D\,panel}(\delta_1, \delta_2) \tag{8}$$

Note that the panel fractions along the chordwise direction of the complete finite wing lattice as well as the respective virtual hinge line positions $\frac{x_{hinge\,\delta_2}}{c}$ for δ_2 have to be identical to the precalculated baseline 2D panel section of eq. 8. In addition the global angle of attack α_∞ affects the discrete vortex solution with normal vector tilt. For that reason the look-up-table has to be precalculated at the same angle of attack as given by the flight condition of the entire finite wing. In principle the these initial calculations for the 2D panel section can be performed once before larger calculation campaigns are launched. Reloading the stored 2D panel data, preferably directly from memory, at the beginning of the respective operating point (α_∞) might save computation time. Unfortunately the modification angles are constrained such that the matrix of the SLE becomes singular when a normal vector is tilted by 90°, i.e. $\delta_1 + \delta_2 = 90°$. However, in practice this limit has never been reached.

Step ①:

The initial solution of the unmodified vortex lattice follows the theory presented in the previous section 3.1 and provides the force vectors $\overrightarrow{F}_i$ acting on each panel.

Step ②:

These forces are integrated along each section to determine the local section lift and pitching moment coefficients $((c_l)_{pot}, (c_m)_{pot})$ delivered by potential theory. The lift coefficient yields

$$(c_l)_{pot} = T_{G \to A} \cdot \frac{1}{qS_{section}} \sum_k \frac{\left(\overrightarrow{F}\right)_k}{(\varepsilon_{CP})_k} \tag{9}$$

where k denotes the panels contained in the processed wing section. $T_{G \to A}$ is the transformation matrix from the global to the aerodynamic coordinate system, q is the dynamic pressure and $S_{section}$ is the section area. Note that the discrete forces $\left(\overrightarrow{F}\right)_k$ have to be corrected for sweep effects if the wing panels have a non-rectangular planform. Since the lift increment depends on the perpendicular distance from the collocation
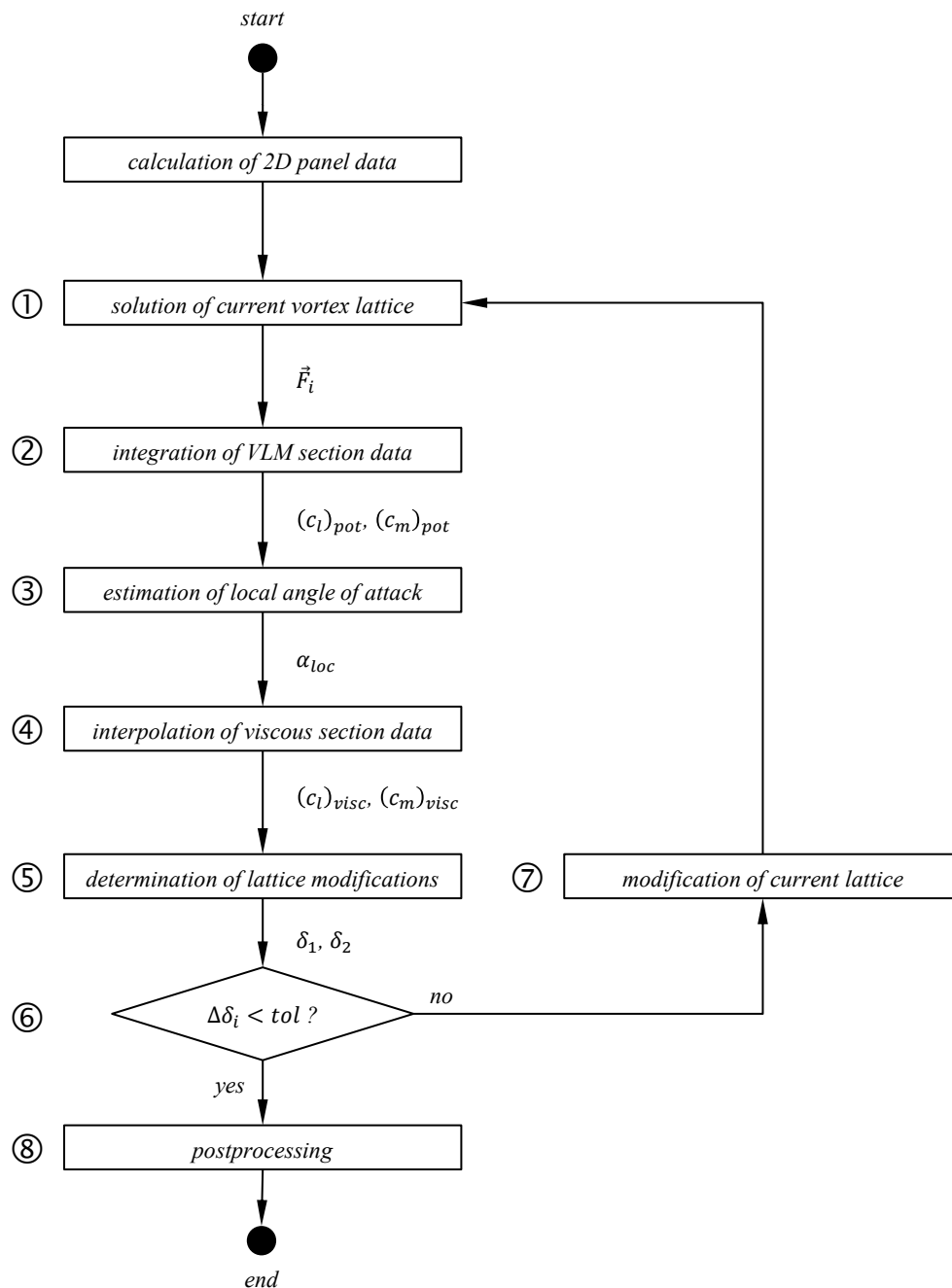
start

●

| *calculation of 2D panel data* |

① | *solution of current vortex lattice* |

$\vec{F}_i$

② | *integration of VLM section data* |

$(c_l)_{pot}, (c_m)_{pot}$

③ | *estimation of local angle of attack* |

α_{loc}

④ | *interpolation of viscous section data* |

$(c_l)_{visc}, (c_m)_{visc}$

⑤ | *determination of lattice modifications* | ⑦ | *modification of current lattice* |

δ_1, δ_2

⑥ ⟨ $\Delta\delta_i < tol$? ⟩   *no*

yes

⑧ | *postprocessing* |

●

end

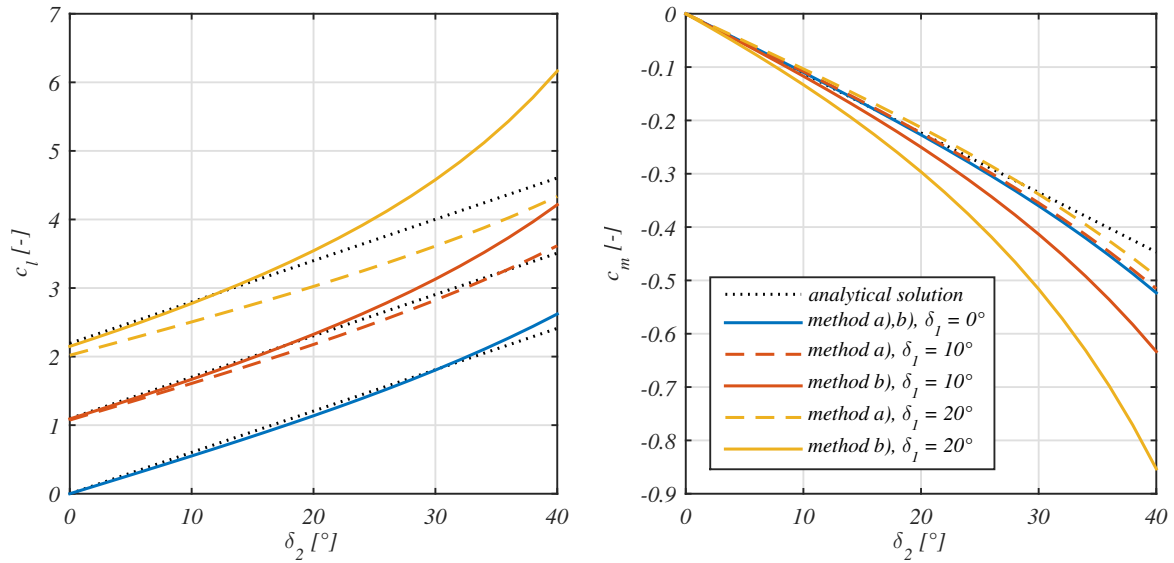**Figure 9: Flow chart of the cambering method calculation process**

Figure 10: Comparison of lift (left) and pitching moment (right) coefficient for the different 2D panel modification methods, $\alpha_\infty = 0°$, $\frac{x_{hinge\,\delta_2}}{c} = 0.8$

point C to the lateral vortex filament AB it changes when the panel is swept. To enable the comparison with the viscous section data the forces are corrected by $(\varepsilon_{CP})_k$ according to the deviation from perpendicularity. The correction factor is based on trigonometric relations and yields

$$\varepsilon_{CP} = \sqrt{1 - \left(\frac{\overrightarrow{r}_{AB} \cdot \overrightarrow{r}_{PC}}{\left\|\overrightarrow{r}_{AB}\right\| \left\|\overrightarrow{r}_{PC}\right\|}\right)^2} \tag{10}$$

Further, the pitching moment coefficient yields

$$(c_m)_{pot} = \frac{1}{qS_{section}c_{section}} \sum_k \frac{\left(\left(\overrightarrow{F}\right)_k \times \Delta \overrightarrow{x}_k\right) \cdot \begin{pmatrix} 0 \\ 1 \\ 0 \end{pmatrix}}{(\varepsilon_{CP})_k} \tag{11}$$

where $c_{section}$ is the mid section chord length and $\Delta\overrightarrow{x}$ the distance from point P to the reference point at the mid section quarter-chord point.

Step ③:

Now the calculated sectional coefficients can be used to estimate the local angle of attack α_{loc} at each section. As the results of $(c_l)_{pot}$ and $(c_m)_{pot}$ from the initial calculations (eq. 8) are monotonic w.r.t. δ_1 and δ_2 (if $\delta_1 + \delta_2 < 90°$) the local angle of attack can be estimated easily by inverse interpolation inside the look-up-tables.

$$(\delta_1^*, \delta_2^*) = f_{2D\,panel}^{-1}\left((c_l)_{pot}, (c_m)_{pot}\right) \tag{12}$$
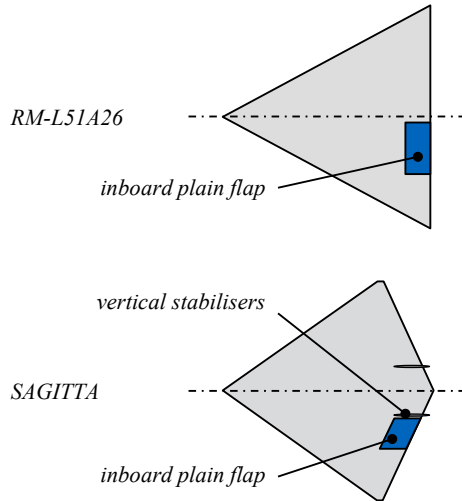
$$\alpha_{loc} = \delta_1^* + \alpha_\infty - \delta_1^{n-1} \tag{13}$$

Step ④:

The viscous section data $(c_l)_{visc}$ and $(c_m)_{visc}$ now can be retrieved by interpolation inside the non-linear viscous data tables that had been obtained by CFD calculations, wind tunnel experiments or other methods

$$(c_l)_{visc} = f_{l_{visc\,data}}(\alpha_{loc}) \tag{14}$$

$$(c_m)_{visc} = f_{m_{visc\,data}}(\alpha_{loc}) \tag{15}$$

Table 1: Specifications of validation test cases

	RM-L51A26 [19]	SAGITTA [20]
planform	*delta*	*diamond*
aspect ratio, AR	2.31	2.0
sweep (LE), $\varphi_{0\%}$	60°	55°
taper ratio, λ	0	~ 0
aerofoil	*NACA 65010*	*NACA 64A012*
Re (M.A.C.)	6.0×10^6	2.2×10^6
flap span fraction	0.25	0.15
reference point, x_{ref}	$0.417 \cdot c_{root}$	$0.25 \cdot c_{MAC}$

Figure 11: Planforms of conventional flap validation test cases

Step ⑤:

Now the vortex lattice can be modified such that the local coefficients of the potential theory solution correspond to the response of the viscous data set. For a high aspect ratio wing with minor 3D effects one would impose the condition $(c_l)_{pot} = (c_l)_{visc}$ and $(c_m)_{pot} = (c_m)_{visc}$ which leads to a new set of angles δ_1^n, δ_2^n for each section after inverse interpolation as already performed before (equ. 12).

$$\left(\delta_1^n, \delta_2^n\right) = f_{2D\,panel}^{-1}\left((c_l)_{visc}, (c_m)_{visc}\right) \tag{16}$$

However, for low aspect ratio wings the associated 3D effects due to flap deflections or equivalent control moment generation induce a virtual additional camber rather than the sole change of local angle of attack. Thus, the local pitching moment increases while the local lift decreases compared to a high aspect ratio wing. This effect also manifests itself in a discrepancy between δ_2^* and δ_2^n on the affected span fractions which usually are expected to be approximately identical when 3D effects are negligible. To account for this the input values of the inverse interpolation (equ. 16) are corrected as follows

$$\left(\delta_1^n, \delta_2^n\right) = f_{2D\,panel}^{-1}\left((c_l)_{visc} + (\Delta c_l)_{corr}, (c_m)_{visc} + (\Delta c_m)_{corr}\right) \tag{17}$$

where the corrections $(\Delta c_l)_{corr}, (\Delta c_m)_{corr}$ are estimated by

$$(\Delta c_l)_{corr} = (c_l)_{pot} - (c_l)_{expected} \tag{18}$$

$$(\Delta c_m)_{corr} = (c_m)_{pot} - (c_m)_{expected} \tag{19}$$

with

$$\left((c_l)_{expected}, (c_m)_{expected}\right) = f_{2D\,panel}\left(\delta_1^*, \delta_2^{n-1}\right) \tag{20}$$

This avoids an overestimation of the viscous section data which is used for the subsequent lattice modification and thus enables the consideration of certain 3D effects for low aspect ratio wings where not only the effective local angle of attack but also the effective camber of the wing sections is affected.

Step ⑥ and ⑦:

If the change in modification angles $\Delta\delta_i = |\delta_i^n - \delta_i^{n-1}|$ compared to the previous iteration exceeds a certain tolerance (e.g. $tol = 0.02°$) the vortex lattice is modified according to the current angles δ_1^n, δ_2^n. For stability reasons it is recommended to use underrelaxation here $\left(\left(\delta_i^n\right)_{applied} = \nu \cdot \delta_i^n + (1 - \nu) \cdot \delta_i^{n-1}\right.$ with e.g. $\nu = 0.8$). Else the results of the last VLM solution are postprocessed to obtain the detailed aerodynamic data.
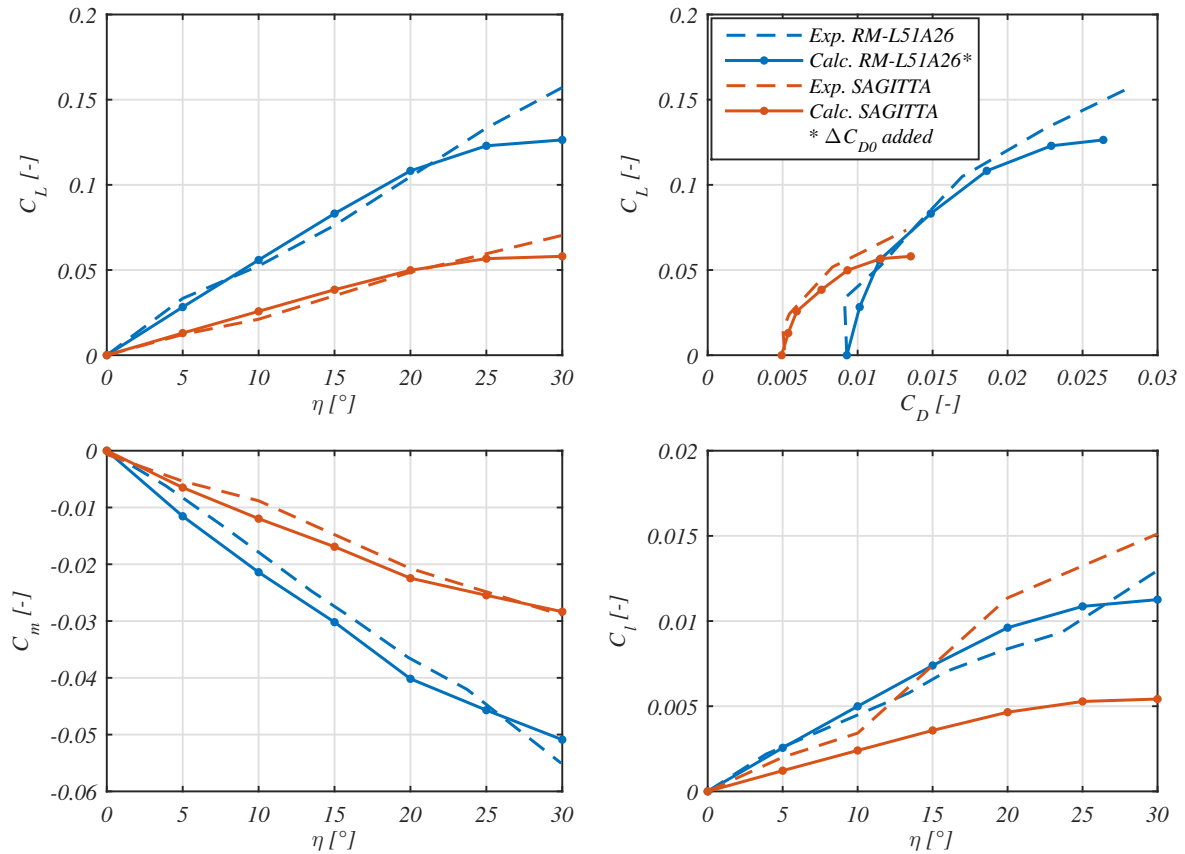
Figure 12: Comparison of numerical results with experimental data for conventional flaps, $\alpha_\infty = 0°, \beta_\infty = 0°$

Step ⑧:

The final postprocessing routine extracts the global force and moment coefficients including coordinate system transformations as well as local parameters along span. Note that the viscous drag retrieved from the viscous section data set $((c_d)_{visc} = f_{d_{visc\,data}}(\alpha_{loc}))$ is added to the induced drag component calculated by vortex lattice theory.

Compared to other methods based on potential theory the applicability of the present method is extended but still restricted. This method of virtual cambering accounts for viscous effects in the subsonic regime that can be modeled in the two-dimensional case. Thus, it is possible to represent zonal separations (e.g. at the wing tips on highly tapered wings) near stall and even in the post-stall regime. Here, studies have shown that smoothing along span of the retrieved viscous data can stabilise the calculation process as the non-linear section data usually does not exhibit a monotonic behaviour (sink) after stall and therefore produces wiggles in the spanwise distributions due to hysteresis effects. However, highly three-dimensional viscous effects like non-linear vortex lift on swept wings cannot be modelled easily by potential theory. Thus, the present method for subsonic flow is restricted to geometries and angles of attack that are not prone to leading edge separation with associated generation of a stable vortex system.

3.3   Validation for Conventional Plain Flaps

The calculation method is validated through comparison of calculated results with the available wind tunnel data of two subsonic test cases. Both low aspect ratio wings are equipped with conventional plain flaps and are characterised by high sweep angles and low taper ratios. The first case comprises a large-scale delta wing having a leading edge sweep angle of $60°$ and an aspect ratio of 2.31 [19]. The SAGITTA diamond wing depicts the second test case having a leading edge sweep angle of $55°$ and an aspect ratio of 2.0 [20, 21]. A summary of further specifications is given in Fig. 11 and Table 1.

Each half span of both vortex lattices were modelled by 20 panels in spanwise direction and 10 panels in chordwise directions. The relative hinge line position of δ_2 in chordwise direction has insignificant impact on the results inside the range of $0.5 \leq \frac{x_{hinge\,\delta_2}}{c} \leq 0.9$ and was set to 0.8. The non-linear viscous 2D data of the baseline aerofoil was calculated by XFOIL [22]. The lift, drag and pitching moment increments through

flap deflection of the two-dimensional section were estimated by a semi-empirical method from ref. [23]. For both cases the iterative calculation process converged after about 10 iterations (RM-L51A26: 9-10 its, SAGITTA: 5-9 its). As can be seen in Fig. 12 lift increments could be predicted quite accurately up to moderate flap deflection angles η. Beyond deflection angles of about $20°$ the numerical results underestimate the lift generation which is due to the semi-empirical method [23] used for the modelling of two-dimensional flap effectiveness. Trailing edge separations at higher flap deflections seem to occur far later in the wind tunnel experiments compared to the semi-empirical model. Also drag prediction exhibits acceptable accuracy. Note that for comparison reasons a drag increment ΔC_{D0} was added to the numerical drag results of the RM-L51A26 case as zero lift drag was underestimated significantly. The pitching moment curves show fairly good agreement between calculated and experimental results except the fact that the semi-empirical underestimation of flap effectiveness beyond $20°$ deflection angle is also present for pitching moment. While the roll moment curves show acceptable agreement for the RM-L51A26 case the SAGITTA curves deviate strongly especially at higher deflection angles. Note that the flap reactions of the SAGITTA wing were measured with mounted vertical stabilisers right next to the flap. The discrepancy could be due to interactions that affect the spanwise lift distribution and thus influence the resulting roll moment.

4   RESULTS OF COMBINED METHODS

The incorporation of the two-dimensional section data (sec. 2) into the cambering method presented in the previous section 3 is demonstrated on the SAGITTA test case for zero angle of attack and zero sideslip ($\alpha_\infty = 0°$, $\beta_\infty = 0°$). The midboard span fraction (Fig. 3) nominally covered by a conventional plain flap is equipped with a Coandă flap featuring a radius-to-chord-ratio of $\frac{r}{c} = 0.02$. The vortex lattice is modelled with the same discretisation parameters as in the previous calculations (sec. 3.3). Fig. 13 shows the aerodynamic forces and moments generated by Coandă flap actuation η_h with a total-slot-height-to-chord-ratio of $\frac{h_{total}}{c} = 0.001$. The different jet velocity ratios $\frac{U_{jet}}{U_\infty}$ correspond to varying total pressure ratios inside the Coandă flap plenum and depend on the operating condition of the used compressor. In accordance with the two-dimensional section data (Fig. 5 and 6) the lift coefficient C_L (Fig. 13a), the pitching moment coefficient C_m (Fig. 13d) and the roll moment coefficient C_l (Fig. 13b) exhibit an approximately linear behaviour for all values of $\frac{U_{jet}}{U_\infty}$. Comparing the effectiveness of the Coandă flap and the nominal conventional flap it can be seen that the jet outflow velocity has to exceed three times the free stream velocity value to attain the same control reactions. Note that the slope of the conventional flap curve depends on the chosen x-axis correlation and has been plotted such that a $30°$ plain flap deflection corresponds to a Coandă flap actuation value of $\eta_h = 1$. Furthermore the curves of pitching moment production efficiency $\frac{C_m}{C_D}$ (Fig. 13e) indicate that there is a chance to attain lower drag values with Coandă flaps than with the conventional flaps even if the jet thrust effect is not included. When incorporating this effect the net force in x-direction is further decreased as depicted by the curves of $C_D - (C_T)_{wing}$ in Fig. 13f where the wing thrust effect coefficient $(C_T)_{wing}$ is defined as

$$(C_T)_{wing} = \frac{\dot{m}\left(V_{jet} - V_\infty\right)}{\frac{1}{2}\rho V_\infty^2} \frac{S_{Coanda\,flap}}{S_{ref}} \tag{21}$$

with $S_{Coanda\,flap}$ denoting the wing area covered by the Coandă aerofoil. As can be seen at high blowing rates ($\frac{U_{jet}}{U_\infty} > 4$) the fluidic flap system generates net thrust, i.e. negative drag for low η_h values.

Fig. 14a shows the spanwise distribution of local lift coefficient including the vortex lattice modification angles δ_1, δ_2 that have been determined iteratively by the proposed calculation method. As expected the curves exhibit increased values at the span fractions that are covered by the Coandă flaps. This can also be seen in Fig. 14b that illustrates the lift and drag fraction ($\frac{c_l c}{C_L c_{avg}}$, $\frac{c_d c}{C_D c_{avg}}$) over span. The drag fraction distribution indicates that a large portion of total drag is produced at the Coandă flap sections where viscous and pressure drag is dominant compared to induced drag ($\frac{(c_d)_i c}{C_D c_{avg}}$).

5   CONCLUSION

A preliminary design method has been presented that translates the two-dimensional aerodynamics of active flow control aerofoils into an aerodynamic data set of a three-dimensional finite wing. A calculation campaign of incompressible 2D RANS calculations on a Coandă aerofoil resulted in a 2D data set containing the aerodynamic reactions due to tangential double-slot-blowing at the rounded trailing edge. Both lift and pitching moment effectiveness exhibit an approximately linear behaviour with the jet outflow ratio η_h between upper and lower slot. The Coandă surface radius ratio $\frac{r}{c}$ as well as the total slot height h_{total} have significant impact
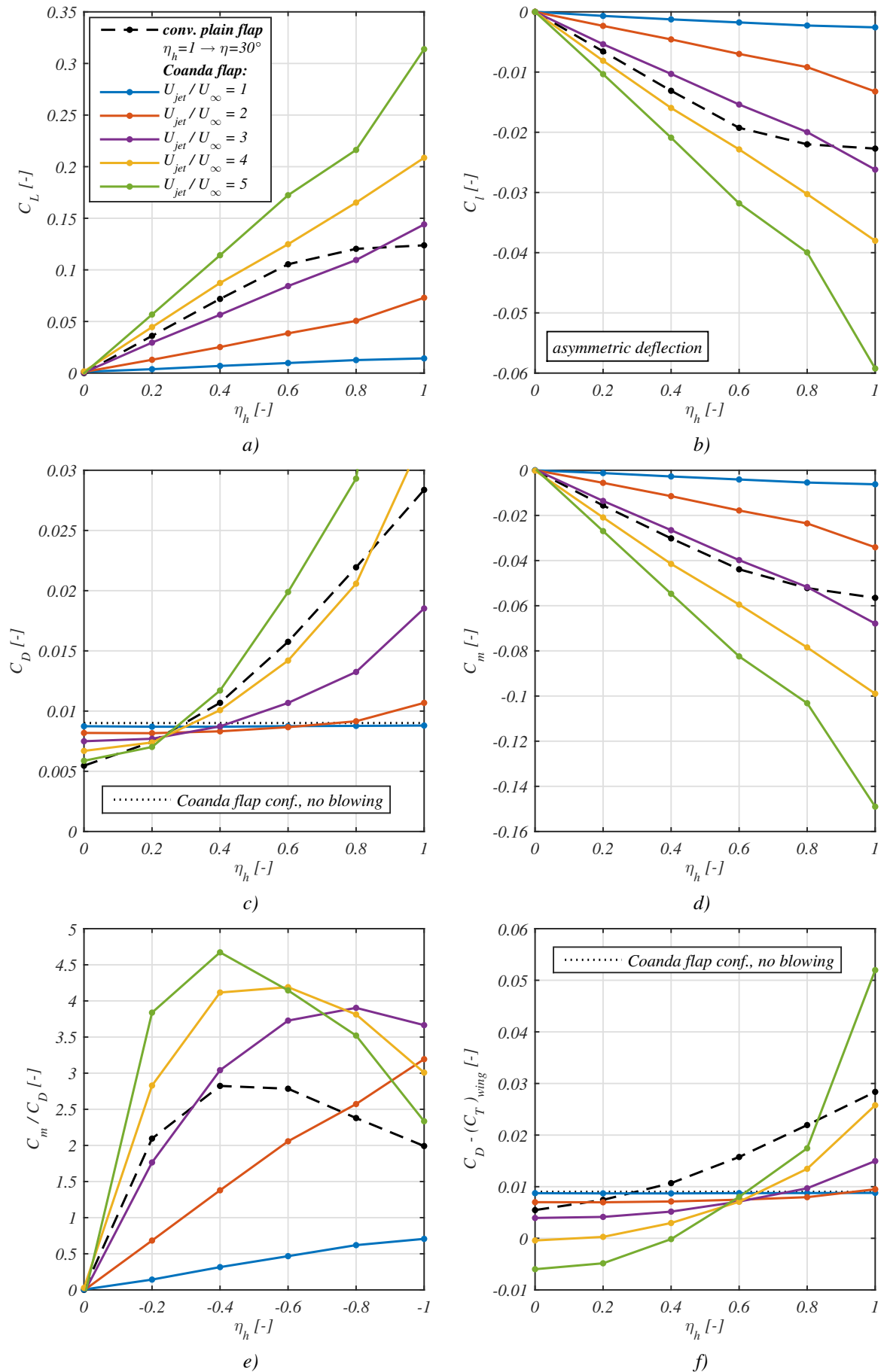
Figure 13: Aerodynamic reactions of the SAGITTA wing due to Coandă flap actuation, $\alpha_\infty = 0°, \beta_\infty = 0°, \frac{h_{total}}{c} = 0.001, \frac{r}{c} = 0.02$
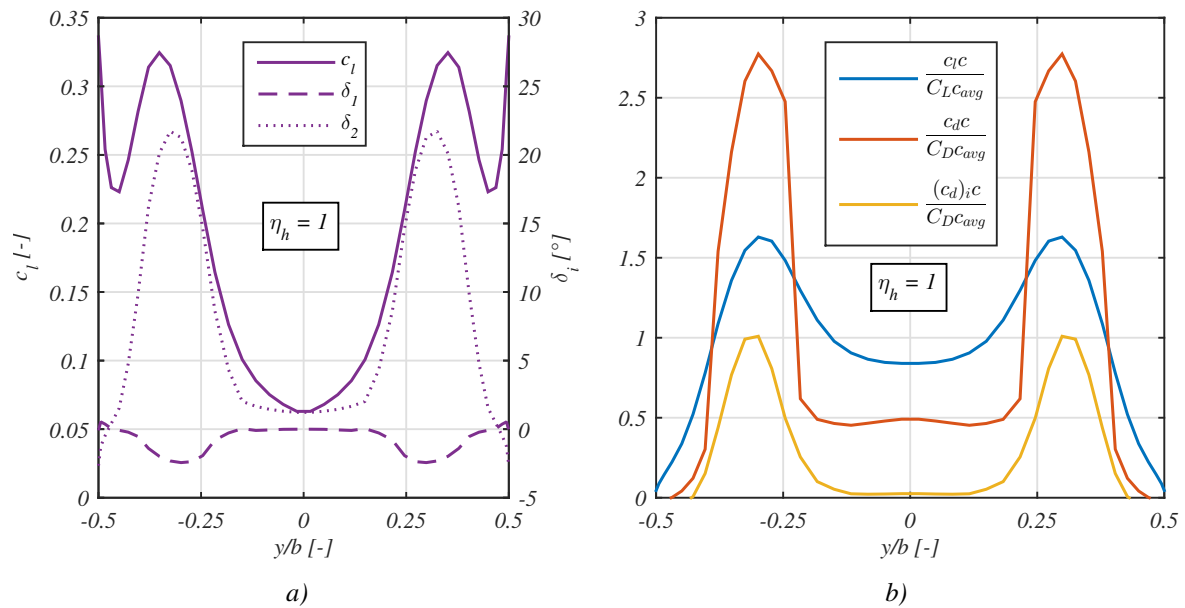
Figure 14: Vortex lattice modification angles over span (a) and span distribution of lift and drag fraction (b), $\frac{U_{jet}}{U_\infty} = 3$, $\alpha_\infty = 0°$, $\beta_\infty = 0°$, $\frac{h_{total}}{c} = 0.001$, $\frac{r}{c} = 0.02$

on control effectiveness and drag, however, with saturated tendency at higher radius and slot sizes. The assembly of this RANS aerofoil data forms the basis for the subsequent extrapolation on the finite wing. A "cambering" method based on potential theory has been described that iteratively modifies the vortex lattice by locally tilting the normal vectors on the collocation points to match the local aerodynamic reactions given by the viscous aerofoil data. An application of the method on low aspect ratio wings with conventional plain flaps showed fairly good agreement between calculated results and measured wind tunnel data. Finally the combination of 2D RANS aerofoil data with the proposed cambering method leads to an aerodynamic data module containing the three-dimensional reactions of the low aspect ratio wing due to Coandă flap actuation. The linear behaviour of Coandă flap control effectiveness with jet outflow momentum ratio η_h persists in the three-dimensional case which is favourable for flight control system design. Calculated total drag values reveal a potential for lower drag generation during Coandă flap actuation compared to the nominal conventional plain flap. However, for a final statement about efficiency the cost due to pressurised air supply (e.g. by engine bleed) have to be taken into account. The benefit or penalty of the Coandă flap system will depend on the flight state of the aircraft. Therefore only a multidisciplinary examination of the intended mission including aerodynamics, flight mechanics and propulsion will give insight into the overall performance of this fluidic flight control system for flapless flight.

References

[1] J. Seifert. SAGITTA - Nationale Forschungskooperation für fortschrittliche UAV-Technologien im Rahmen der Open Innovation Initiative von Cassidian. In *61. Deutscher Luft- und Raumfahrtkongress der Deutschen Gesellschaft für Luft- und Raumfahrt e.V.*, 2012.

[2] R. J. Englar. Two-Dimensional Transonic Wind Tunnel Tests of Three 15-Percent Thick Circulation Control Airfoils. Technical Report AD882075, David W. Taylor Naval Ship Research and Development Center, 1970.

[3] J. Abramson. Characteristics of a Cambered Circulation Control Airfoil Having Both Upper and Lower Surface Trailing Edge Slots. Technical report, Naval Surface Warfare Center, Carderock Division, West Bethesda, 2004.

[4] S. Frith and N. Wood. Investigation of Dual Circulation Control Surfaces for Flight Control. In *2nd AIAA Flow Control Conference*, Fluid Dynamics and Co-located Conferences. American Institute of Aeronautics and Astronautics, 2004.

[5] M. G. Alexander, S. G. Anders, S. K. Johnson, J. P. Florance, and D. F. Keller. Trailing Edge Blowing

on a Two-Dimensional Six-Percent Thick Elliptical Circulation Control Airfoil Up to Transonic Conditions: NASA/TM-2005-213545. Technical report, NASA Langley Research Center, Langley and USA, 2005.

[6] G. Jones, C.-S. Yao, and B. Allan. Experimental Investigation of a 2D Supercritical Circulation-Control Airfoil Using Particle Image Velocimetry. In *3rd AIAA Flow Control Conference*, Fluid Dynamics and Co-located Conferences. American Institute of Aeronautics and Astronautics, 2006.

[7] K. Stadlberger and M. Hornung. Design Drivers for Novel Flight Control Effectors for Low Aspect Ratio Flying-Wing Configurations. In *61. Deutscher Luft- und Raumfahrtkongress der Deutschen Gesellschaft für Luft- und Raumfahrt e.V.*, 2012.

[8] R. Mukherjee and A. Gopalarathnam. Poststall Prediction of Multiple-Lifting-Surface Configurations Using a Decambering Approach. *Journal of Aircraft*, 43(3):660–668, 2006.

[9] K. Stadlberger and M. Hornung. Challenges in the Modelling of Blown Circulation Control Aerofoils. In *63. Deutscher Luft- und Raumfahrtkongress der Deutschen Gesellschaft für Luft- und Raumfahrt e.V.*, 2014.

[10] D. B. Spalding. A novel finite difference formulation for differential expressions involving both first and second derivatives. *International Journal for Numerical Methods in Engineering*, 4(4):551–559, 1972.

[11] F. H. Harlow and J. E. Welch. Numerical Calculation of Time–Dependent Viscous Incompressible Flow of Fluid with Free Surface. *Physics of Fluids (1958-1988)*, 8(12):2182–2189, 1965.

[12] F. R. Menter, M. Kuntz, and R. Langtry. Ten Years of Industrial Experience with the SST Turbulence Model. *Turbulence, Heat and Mass Transfer*, (4):625–632, 2003.

[13] L. Prandtl. Applications of modern hydrodynamics to aeronautics. Technical Report 116, Universität Göttingen, 1923.

[14] V. M. Falkner. The Scope and Accuracy of Vortex Lattice Theory. Technical Report 2740, Ministry of Supply, Aeronautical Research Council, London, 1952.

[15] J. C. Sivells and R. H. Neely. Method for calculating wing characteristics by lifting-line theory using nonlinear section lift data. Technical Report TN1269, Langley Aeronautical Laboratory, 1947.

[16] Anderson, J. D. and S. Corda. Numerical lifting line theory applied to drooped leading-edge wings below and above stall. *Journal of Aircraft*, 17(12):898–904, 1980.

[17] W. F. Phillips and D. O. Snyder. Modern Adaptation of Prandtl's Classic Lifting-Line Theory. *Journal of Aircraft*, 37(4):662–670, 2000.

[18] J. Katz and A. Plotkin. *Low speed aerodynamics*, volume 13 of *Cambridge aerospace series*. Cambridge University Press, Cambridge and UK and New York, 2nd ed edition, 2001.

[19] J. G. Hawes and May Jr, Ralph W. Investigation at Low Speed of the Effectiveness and Hinge Moments of a Constant-Chord Ailavator on a Large-Scale Triangular Wing with Section Modification. Technical Report RM-L51A26, Langley Aeronautical Laboratory, 1951.

[20] A. Hövelmann, S. Pfnür, and C. Breitsamter. Flap Efficiency Analysis for the SAGITTA Diamond Wing Demonstrator Configuration. In *63. Deutscher Luft- und Raumfahrtkongress der Deutschen Gesellschaft für Luft- und Raumfahrt e.V.*, 2014.

[21] A. Hövelmann and C. Breitsamter. Aerodynamic Characteristics of the SAGITTA Diamond Wing Demonstrator Configuration. In *61. Deutscher Luft- und Raumfahrtkongress der Deutschen Gesellschaft für Luft- und Raumfahrt e.V.*, 2012.

[22] M. Drela. XFOIL: An Analysis and Design System for Low Reynolds Number Airfoils. In *Low Reynolds Number Aerodynamics*, volume 54 of *Lecture Notes in Engineering*, pages 1–12. Springer Berlin Heidelberg, 1989.

[23] R. Fink. USAF Stability and Control DATCOM. Technical Report AFWAL-TR-83-3048, McDonnell Douglas Corporation, Long Beach and California and USA, 1978.